 DOI: 10.1086/662670

Appendix A from N. Mideo et al., "Causes of Variation in Malaria Infection Dynamics: Insights from Theory and Data"

(Am. Nat., vol. 178, no. 6, p. 174)

Supplementary Methods

Effects of Experimental Manipulation

Some effects of our experimental manipulation of host immunity and RBC age structure can be seen in figure A1. Mean parasite densities for each treatment over the initial peak of infection are shown in figure A1, top row. As expected, parasite densities are higher in $CD4^+$ T-depleted mice than in immune-intact control mice (Barclay et al. 2008). Mean RBC densities for each treatment over the initial peak of infection are shown in figure A1, bottom row. PHZ treatment results in a marked decrease in RBC densities. Figure A2 illustrates that PHZ-treated mice had significantly higher proportions of bloodstream reticulocytes and that a significantly higher proportion of infected RBCs were reticulocytes, across the relevant days postinfection.

Model Derivation

Basic Structure

Incorporating the age structure of the Mideo et al. (2008*b*) model into the model of Miller et al. (2010) yields the following basic model structure. On the $(i+1)$th day postinfection, just after all infected red blood cells (RBCs) burst, the densities of merozoites, M_{i+1}, reticulocytes on their jth day in the bloodstream, $R_{j,i+1}$, and mature RBCs, N_{i+1} are given by

$$\begin{aligned}
M_{i+1} &= \omega_{\mathrm{R}} \sum_{j=1}^{3} R_{j,i}[\lambda_{\mathrm{R}} e^{(\lambda_{\mathrm{R}}+d+I_{\mathrm{p},i})} + (1-e^{-\lambda_{\mathrm{R}}})e^{-(d+d_2+I_{\mathrm{p},i})}] \\
&\quad + \omega_{\mathrm{N}} N_i[\lambda_{\mathrm{N}} e^{(\lambda_{\mathrm{N}}+d+I_{\mathrm{p},i})} + (1-e^{-\lambda_{\mathrm{N}}})e^{-(d+d_2+I_{\mathrm{p},i})}], \\
R_{1,i+1} &= [\theta(K-T_{i-r}) + dK]\frac{1-e^{-(d+I_{\mathrm{u},i})}}{d+I_{\mathrm{u},i}}, \\
R_{2,i+1} &= R_{1,i} e^{-(\lambda_{\mathrm{R}}+d+I_{\mathrm{u},i})}, \\
R_{3,i+1} &= R_{2,i} e^{-(\lambda_{\mathrm{R}}+d+I_{\mathrm{u},i})}, \\
N_{i+1} &= R_{3,i} e^{-(\lambda_{\mathrm{R}}+d+I_{\mathrm{u},i})} + N_i e^{-(\lambda_{\mathrm{N}}+d+I_{\mathrm{u},i})},
\end{aligned}$$

where ω_{R} and ω_{N} are the number of progeny parasites produced in infected reticulocytes and mature RBCs, respectively, K is the normal total RBC density in the absence of infection and natural death, θ is the proportion of any RBC deficit that is made up in one day (and describes how RBC production increases with anemia; we therefore refer to it as the "upregulation rate"), d is the natural death rate of RBCs, d_2 is the additional death rate of multiply-parasitized RBCs and $T_{i-\tau} = \sum_{j-1}^{3} R_{j,i-\tau} + N_{i-\tau}$ is the total RBC density τ days before i. The parameter τ allows RBC production in response to anemia to be time-lagged, since RBC precursors take time to develop in the bone marrow. The parameters $I_{\mathrm{p},i}$ and $I_{\mathrm{u},i}$ describe the immune clearance rates of parasitized and unparasitized RBCs as a function of time i. These parameters are described in more detail below. The parameters λ_{R} and λ_{N} define the average number of merozoites (that survive clearance in the bloodstream) per reticulocyte

and mature RBC, respectively. To find expressions for these parameters, we note that an individual merozoite has a probability of infecting a reticulocyte given by

$$\frac{\beta_{\mathrm{R}} \sum_{i=1}^{3} R_{j,i}}{\beta_{\mathrm{R}} \sum_{j=1}^{3} R_{j,i} + \beta_{\mathrm{N}} N_i + \mu + I_{\mathrm{m},i}},$$

and an individual merozoite has a probability of infecting a mature RBC given by

$$\frac{\beta_{\mathrm{N}} N_i}{\beta_{\mathrm{R}} \sum_{j=1}^{3} R_{j,i} + \beta_{\mathrm{N}} N_i + \mu + I_{\mathrm{m},i}},$$

where β_{R} and β_{N} are the invasion rates of reticulocytes and mature RBCs, μ is the death rate of merozoites in the bloodstream, and $I_{\mathrm{m},i}$ describes the immune clearance rate of merozoites as a function of time, i. Multiplying these probabilities by the initial density of merozoites and dividing by the respective densities of RBCs gives the average number of merozoites per reticulocyte:

$$\lambda_{\mathrm{R}} = \frac{\beta_{\mathrm{R}} M_i}{\beta_{\mathrm{R}} \sum_{j=1}^{3} R_{j,i} + \beta_{\mathrm{N}} N_i + \mu + I_{\mathrm{m},i}}$$

and the average number of merozoites per mature RBC

$$\lambda_{\mathrm{N}} = \frac{\beta_{\mathrm{N}} M_i}{\beta_{\mathrm{R}} \sum_{j=1}^{3} R_{j,i} + \beta_{\mathrm{N}} N_i + \mu + I_{\mathrm{m},i}}.$$

The probability of a reticulocyte being infected by k merozoites is Poisson distributed with parameter λ_{R} and the probability of a mature RBC being infected by k merozoites is Poisson distributed with parameter λ_{N} (Miller et al. 2010). See Miller et al. (2010) for further details on the derivation of the model without age structure.

The model of Mideo et al. (2008*b*) discussed in the main text is recovered by setting all immune clearance parameters ($I_{\mathrm{m},i}$, $I_{\mathrm{p},i}$, and $I_{\mathrm{u},i}$) to 0. This is slightly different than the published model in Mideo et al. (2008*b*) since it tracks infections in time steps of thirds of a day rather than whole days and multiply infected RBCs are tracked separately. This allows the model to make predictions about the densities of unparasitized, singly parasitized, and multiply parasitized cells that should more accurately correspond to what is measured experimentally. However, all underlying biological hypotheses described by the model remain unchanged.

Immune Clearance

Three independent functions describe the immune clearance rates of merozoites, parasitized RBCs, and unparasitized RBCs over the course of infection (denoted $I_{\mathrm{m},i}$, $I_{\mathrm{p},i}$, and $I_{\mathrm{u},i}$). We assume that there are at maximum two "windows" of immune activity, and each window is described by four parameters (so each function is fully described by eight parameters). A schematic "clearance rate function" for parasitized RBCs is given in figure 1 of the main text. The parameter s_x defines the day postinfection when immune clearance begins, c_x represents the maximum clearance rate, r_x represents the time it takes to reach that maximum rate (or "rise time"), and l_x represents the duration of immune clearance (note that $r_x \leq l_x$). The subscript x denotes the cells being cleared (either m for merozoites, p for parasitized RBCs, or u for unparasitized RBCs). For each immune clearance function, the two windows of immune activity will be described by a different set of parameters.

Model Fitting

The fitted model parameters and prior distributions are given in table A1. The prior distributions were either taken from the literature or based on our experimental measurements. The prior distributions for burst size, RBC upregulation rate, and invasion rate are specified with hyperparameters (table A2); hyperparameters essentially specify the distribution from which the individual-level parameters are randomly drawn. We do this for these parameters because we want to examine if they are parasite genotype-specific (see below).

As well as fitting the hybrid model (Mideo et al. 2008*b*; Miller et al. 2010) with age structure and immune responses, we fit a model without age structure (Miller et al. 2010) by setting reticulocyte and normocyte burst sizes and invasion rates equal ($\omega = \omega_{\mathrm{N}} = \omega_{\mathrm{R}}$, $\beta = \beta_{\mathrm{N}} = \beta_{\mathrm{R}}$) and a model without immune responses (Mideo et

al. 2008*b*) by setting immune-mediated clearance rates to 0 ($c_m = c_p = c_u = 0$). We also fit models without age structure and with each of the three immune components removed by setting their respective clearance rates to 0.

Miller et al. (2010) showed that there is a nonidentifiability between RBC invasion rate β and natural death rate of merozoites μ. This meant that it was impossible to obtain separate estimates for them and all that could be obtained was their ratio. In Mideo et al. (2008*b*), however, we did not fit μ but assumed it had a value of 48 d^{-1}; thus, an estimate for β was obtainable. In order to test for genotype-specific differences in invasion rates we must therefore fix μ and assume that it is non-genotype-specific. Miller et al. (2010) estimated μ/β to be of the order 10^6, taking $\mu = 48$ as in Mideo et al. (2008*b*) gives β^{-1} to be of the order 10^4. The inverse of β is estimated rather than β because we have no prior knowledge about its upper bound.

In order to determine if there are genotype-specific differences in parameters we estimate the hyperparameters of the two strains in the model without age structure. For example, the prior distribution of burst size for AS-infected mice is $N(\nu_{\omega,\mathrm{AS}}, \sigma_\omega^2)$ and for DK-infected mice $N(\nu_{\omega,\mathrm{DK}}, \sigma_\omega^2)$. Terms $\nu_{\omega,\mathrm{AS}}$, $\nu_{\omega,\mathrm{DK}}$, σ_ω^2 are hyperparameters that we estimate. If there are genotype specific differences in parameter estimates we expect to see a difference in the posterior distributions of $\nu_{\omega,\mathrm{AS}}$ and $\nu_{\omega,\mathrm{DK}}$, that is, the mean burst sizes of mice infected with AS and DK parasites, respectively. The variance hyperparameter σ_ω^2, is assumed to be non-strain-specific as it is of little interest here. We can also suppose that the burst sizes for all mice are randomly drawn from the same population, that is, non-strain-specific burst sizes, which means we take the prior as $N(\nu_\omega, \sigma_\omega^2)$ over all mice. We must also specify hyperpriors on the hyperparameters; these are given in table A2 and are chosen to be conjugate to the priors.

By estimating genotype-specific and non-genotype-specific hyperparameters we can calculate the (marginalized) likelihood ratio of the data supposing genotype-specific hyperparameters to the data supposing non-genotype-specific hyperparameters. Without any prior preference for these two suppositions their prior odds are 1 : 1. Thus, by Bayes's theorem, our posterior odds for these suppositions are equal to their likelihood ratio. If $\Pr(D_m|M)$ is the likelihood of mouse m's data given model M, then our odds on genotype-specific hyperparameters is given by the ratio

$$\frac{\Pi_m \Pr(D_m|\text{genotype-specific hyperparameters})}{\Pi_m \Pr(D_m|\text{nongenotype-specific hyperparameters})}.$$

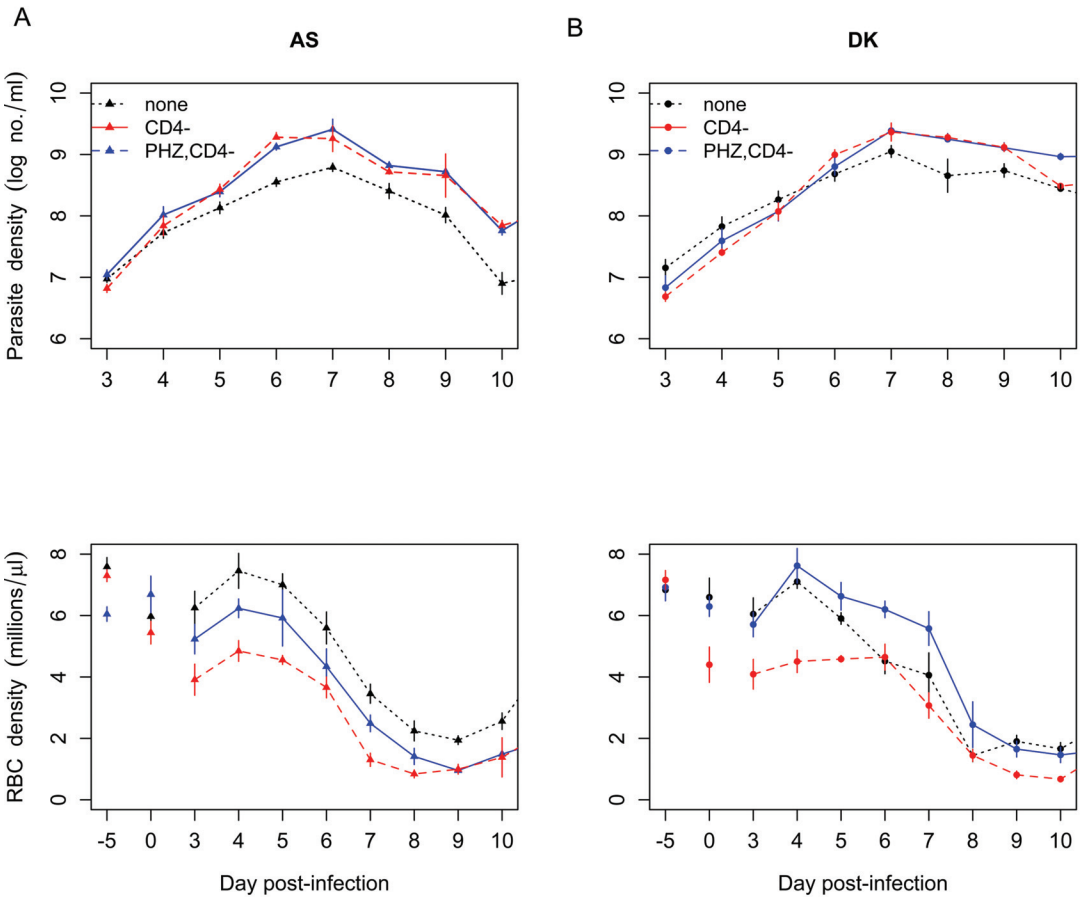

Figure A1: Infection dynamics of different treatments. Treatments are grouped by parasite genotype: *A*, More virulent parasite genotype AS; *B*, less virulent parasite genotype DK. Top row shows mean parasite density, and bottom row shows mean RBC densities over time. Error bars, ± 1 SEM. Colors indicate what treatments in addition to infection the hosts received: black, none (immune-intact control); blue, $CD4^+$ depletion (CD4−); red, PHZ and $CD4^+$ depletion. Over the course of the initial peak, parasite densities were higher in $CD4^+$-depleted hosts as compared with immune-intact hosts. PHZ treatment (2 days before infection, i.e., day -2) resulted in a decrease in red blood cell densities. This effect coincided with the initial stages of infection.

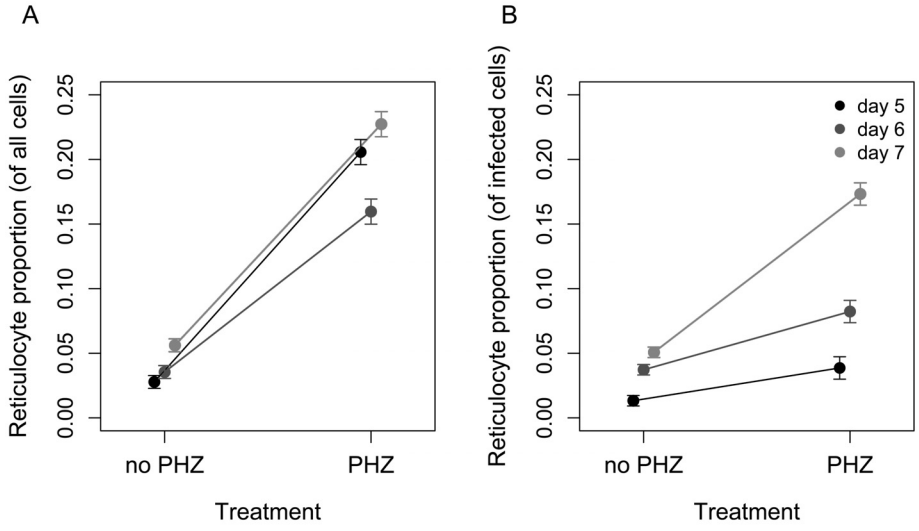

Figure A2: Effect of phenylhydrazine (PHZ) on red blood cell age structure in $CD4^+$ depleted mice. The mean proportion of all red blood cells (RBCs) that are reticulocytes (*A*) and infected RBCs that are reticulocytes (*B*) over 3 consecutive days in untreated mice and those that received PHZ treatment. Error bars, ± 1 SEM. At the early stages of infection, mice treated with PHZ had a significantly higher proportion of reticulocytes, as expected, and subsequently, a significantly higher proportion of all infected cells were also reticulocytes.

Table A1. Model parameters and prior distributions of hybrid model

Parameter	Description	Value or prior	Source
ω_R, ω_N	Burst sizes in reticulocytes and normocytes	$N(\nu_\omega, \sigma_\omega^2)$	See table A2
β_R, β_N	Invasion rate of reticulocytes, normocytes ([cells/μL]$^{-1}$ s^{-1})	Not fitted	
ρ	$\log_{10}(\beta_R/\beta_N)$	$N(0, .3^2)$	Hetzel and Anderson 1996; Antia et al. 2008; Mideo et al. 2008*b*
μ	Natural death rate of merozoites (day^{-1})	48	Garnham 1966; Mideo et al. 2008*b*
β^{-1}	Inverse of invasion rate (cells s/μL)	Exp(l)	See table A2
θ	Rate of upregulation of erythropoeisis (day^{-1})	$N(\nu_\theta, \sigma_\theta^2)$	See table A2
τ	Time lag in erythropoeisis (day)	$U(0, 6)$	Chang et al. 2004; Mideo et al. 2008*b*
d	Natural death rate of RBCs (day^{-1})	.025	van Putten 1958; Bannerman 1983
d_m	Increased death rate of multiply-parasitized RBCs (day^{-1})	Exp(1)	Miller et al. 2010
s_m, s_p, s_u	Start day of immunity targeting merozoites, parasitized RBCs, unparasitized RBCs	$U(0, 21)$	Miller et al. 2010
r_m, r_p, r_u	Rise time of immunity targeting merozoites, parasitized RBCs, unparasitized RBCs	$U(0, 21)$	Miller et al. 2010
c_m	Maximum level of immunity targeting merozoites (cells/s)	Exp(10^8)	Miller et al. 2010
c_p, c_u	Maximum clearance rate of immunity targeting parasitized RBCs, unparasitized RBCs (day^{-1})	Exp(1)	Miller et al. 2010
l_m, l_p, l_u	Duration of immunity targeting merozoites, parasitized RBCs, unparasitized RBCs	$U(0, 21)$	Miller et al. 2010
P_0	Initial parasite density (parasites/μL)	$\log N(1.5, .5^2)$	Miller et al. 2010
N_0	Initial RBC density (RBCs/μL)	$N_T(6.5 \times 10^6, 10^{12})$	

Note: RBC = red blood cell.

Table A2. Hyperparameters and their hyperprior distributions.

Hyperparameter	Description	Hyperprior	Source
ν_ω	Mean burst size	$N(6, .5^2)$	Garnham 1966; Carter and Walliker 1975; Carter and Diggs 1977; Mideo et al. 2008*b*
σ_ω^2	Variance of burst size	InvGam(2, 1^2)	Garnham 1966; Carter and Walliker 1975; Carter and Diggs 1977; Mideo et al. 2008*b*
ν_β	Mean inverse invasion rate	InvGam(1, 10^4)	Mideo et al. 2008*b*
ν_θ	Mean red blood cell upregulation rate	$N(0.4, 0.2^2)$	Haydon et al. 2003; Mideo et al. 2008*b*
σ_θ^2	Variance of red blood cell upregulation rate	InvGam(2, 0.2^2)	Haydon et al. 2003; Mideo et al. 2008*b*

 DOI: 10.1086/662670

Appendix B from N. Mideo et al., "Causes of Variation in Malaria Infection Dynamics: Insights from Theory and Data"

(Am. Nat., vol. 178, no. 6, p. 174)

Supplementary Results

Statistical Analyses of Experimental Data

Tables B1 and B2 present statistics from linear mixed effects models of invasion rate variation and linear models of burst size variation. Histograms showing the burst size observations across treatment groups are shown in figure B1.

Assessing Model "Goodness of Fit"

We compare the fit of our original model (Mideo et al. 2008*b*) with that of the hybrid model, which includes multiple forms of immunity, by plotting the overlaid standardized residuals for parasite and RBC densities for each model (fig. B2). When the mean of the standardized residuals lies outside the 95% (Bonferroni corrected for multiple tests) predictive interval (i.e., the red line falls outside of the dashed lines), this suggests that the model is over- or underestimating the data, and is suggestive of a poor fit. While there are clearly some time points for which neither model captures the data well, overall the hybrid model is fitting better (fig. B2, *right*). The early time points for which the RBC densities are fitted poorly is not particularly surprising since there is a lot of unexplained variation in the data at these very early days postinfection.

Model Inferences

The most likely model includes immune responses that independently target merozoites, parasitized RBCs, and unparasitized RBCs, although not every response is necessary to explain the dynamics of every individual mouse. This individual variation is evident in the posterior predictive intervals for the different immune responses, depicted below (figs. B3–B5). Overall, immune responses targeting merozoites and parasitized RBCs are more important for explaining the dynamics of infections with the more virulent clone AS than with the less virulent clone DK. The marginal posterior distributions for all other parameters are given in figure B6.

Refitting Original Data

Given that the model we presented in Mideo et al. (2008*b*) was assessed as providing a "good fit" to the data used in that study, we refit that data (originally from Barclay et al. 2008) to the Mideo et al. (2008*b*) model and the Miller et al. (2010) model using the Bayesian framework of this study. As with the new data we explore in the main text, the immune response is necessary to explain the data from infections with the more virulent genotype, but not the avirulent genotype (table B3).

In figure B6, we compare the best fits from Mideo et al. (2008*b*), where models were fitted only to parasite data, with the new hybrid model fitted to this same data.

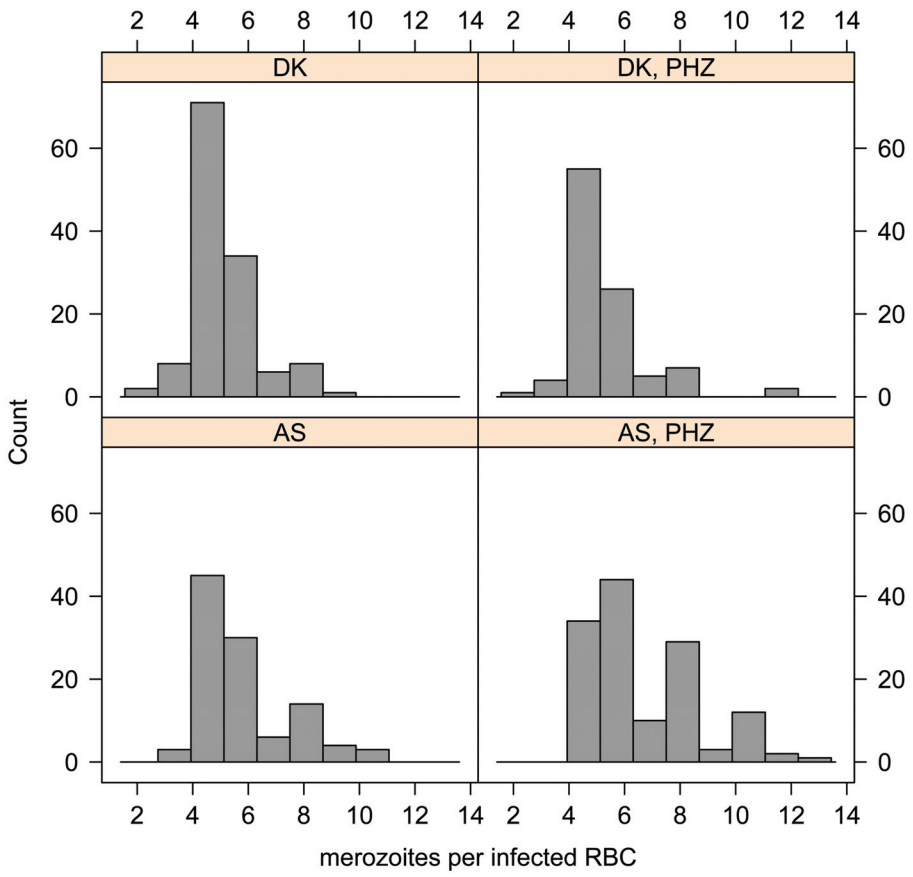

Figure B1: Histogram of burst size observations across treatments. Burst sizes were estimated by counting the number of merozoites in at least 25 mature schizonts for each individual infected mouse. The distributions here are plotted from pooling this data according to the genotype of the infecting parasites (DK or AS) and phenylhydrazine treatment (PHZ or none).

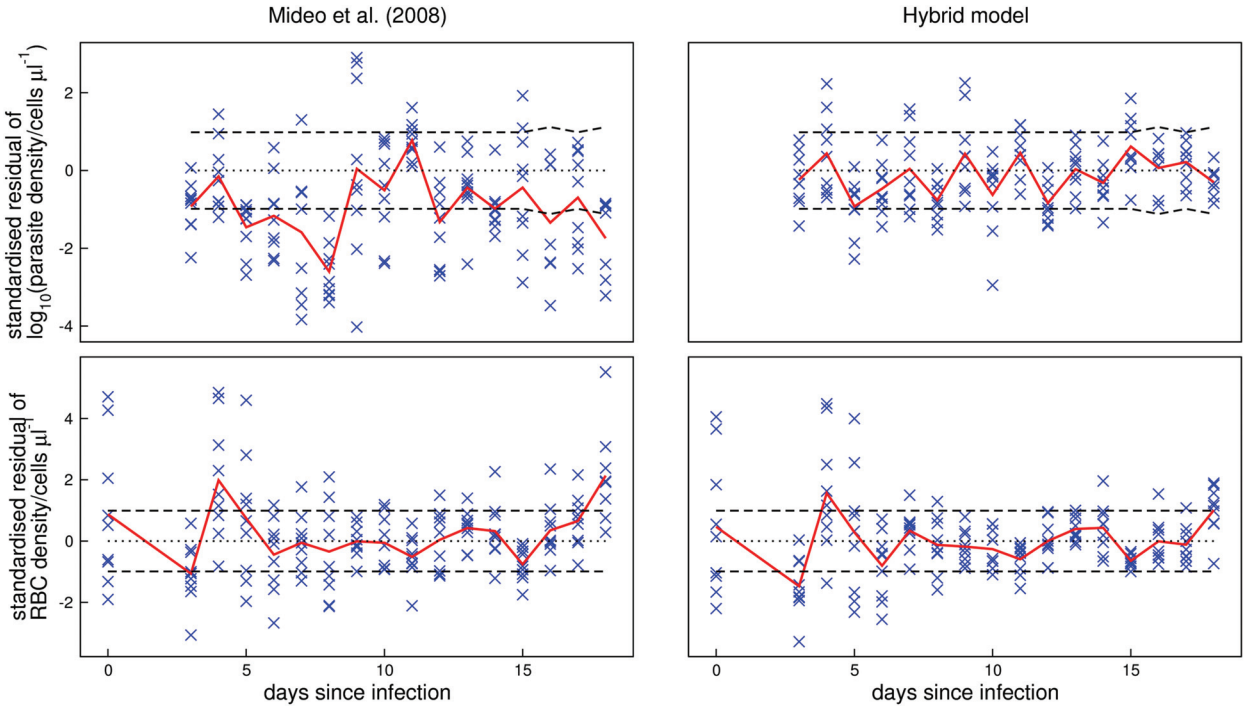

Figure B2: Standardized residuals of the fit of the age-structured model of Mideo et al. (2008*b*; *left*) and the fit to the hybrid model (*right*) to newly collected data. *Top*, Parasite density; *bottom*, red blood cell density. Each cross represents the standardized residual on a particular day for an individual mouse. The red line joins the means of the standardized residuals for each day, and the dashed lines denote the 95% (Bonferroni corrected for multiple tests) predictive intervals of the mean standardized residual assuming the model is true. The *Y*-axis is scaled to units of standard deviations.

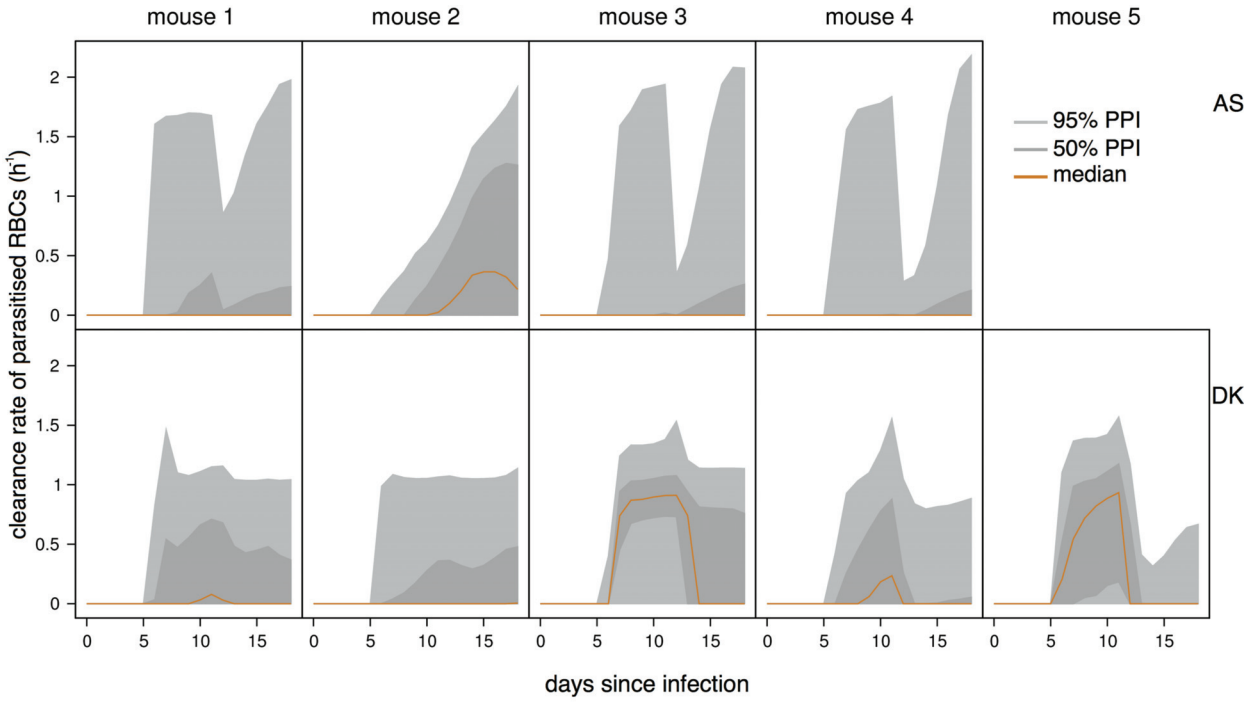

Figure B3: Posterior predictive interval (PPI) of immune responses targeting parasitized red blood cells (RBCs). Solid lines give best-fit function describing clearance rate. Light gray regions correspond to 95% PPI; dark gray regions correspond to 50% PPI.

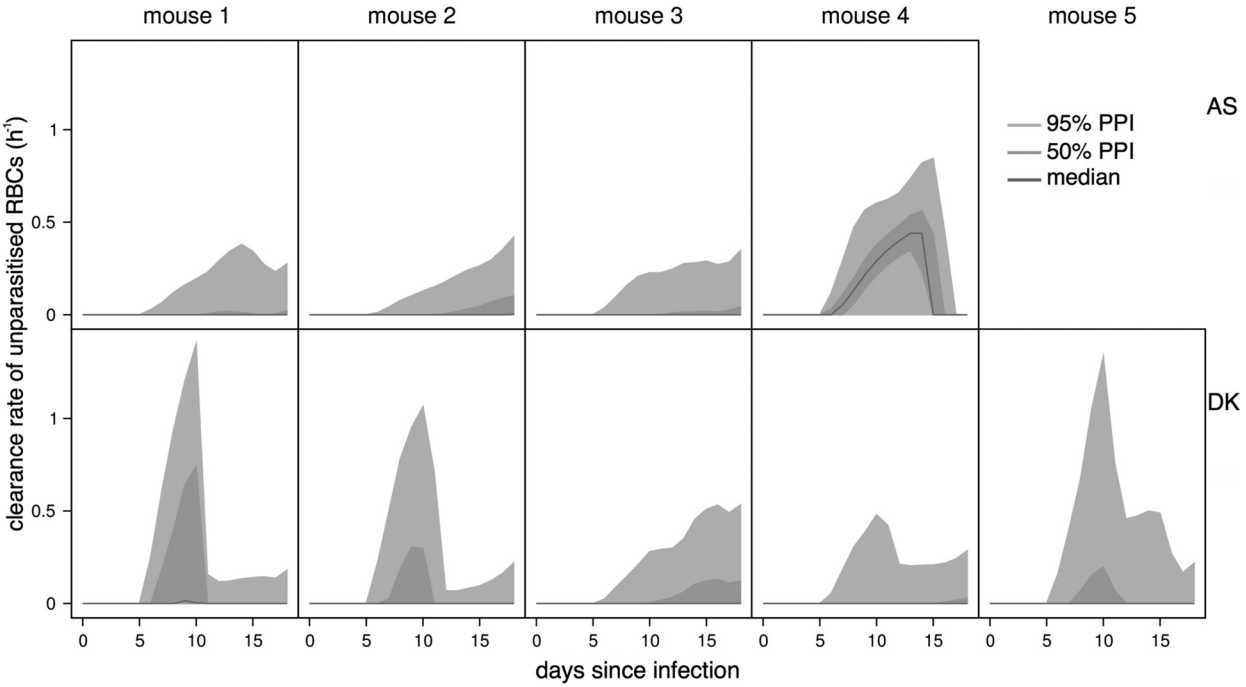

Figure B4: Posterior predictive interval (PPI) of immune responses targeting unparasitized red blood cells (RBCs; i.e., bystander death). Solid lines give best-fit function describing clearance rate. Light gray regions correspond to 95% PPI; dark gray regions correspond to 50% PPI.

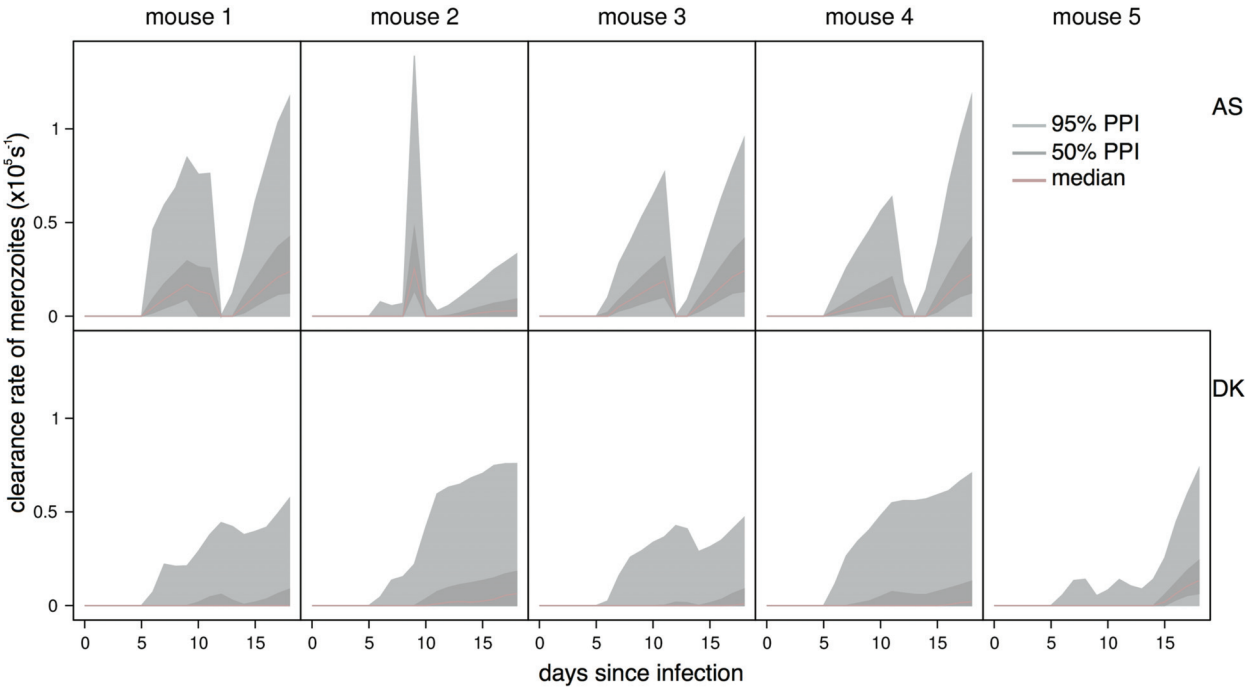

Figure B5: Posterior predictive interval (PPI) of immune responses targeting merozoites. Solid lines give best-fit function describing total clearance. Light gray regions correspond to 95% PPI; dark gray regions correspond to 50% PPI.

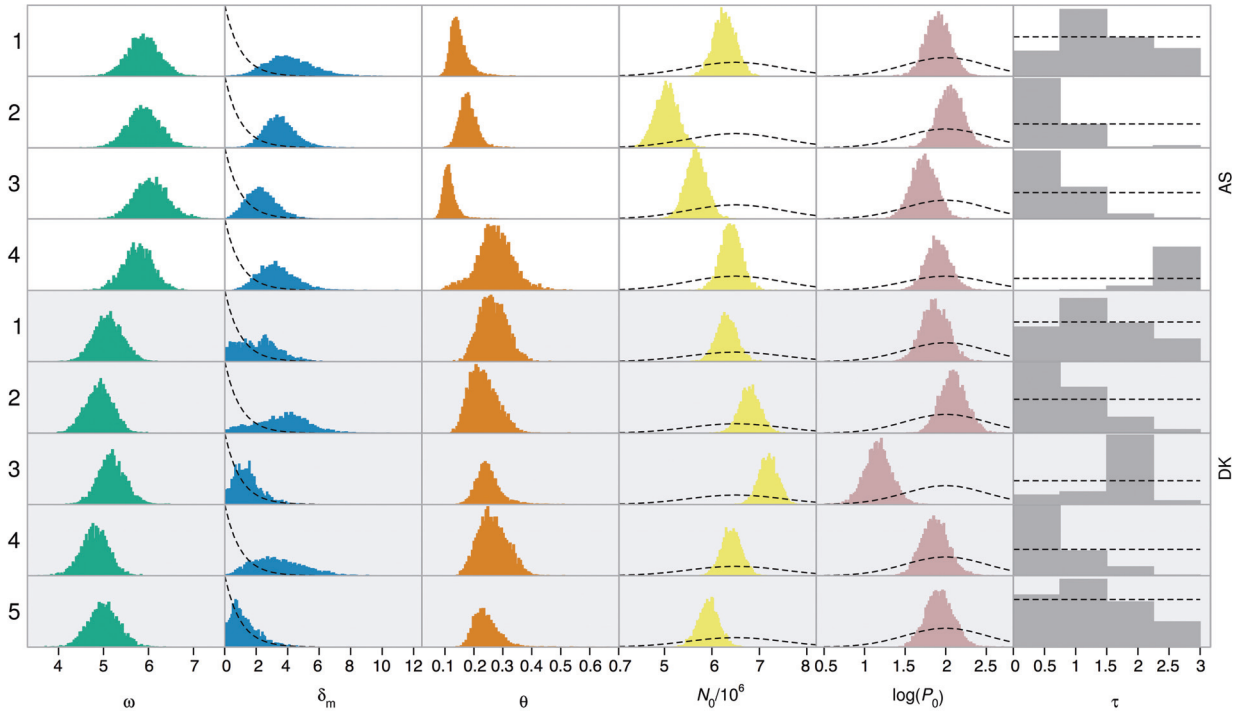

Figure B6: Marginal distributions of fitted parameters for the most likely reduced hybrid model. Each row corresponds to an individual mouse. White panels are for individuals infected with the more virulent genotype AS; gray panels are for individuals infected with the less virulent genotype DK. Dashed lines indicate the prior distributions on each parameter. Units are given in table A1.

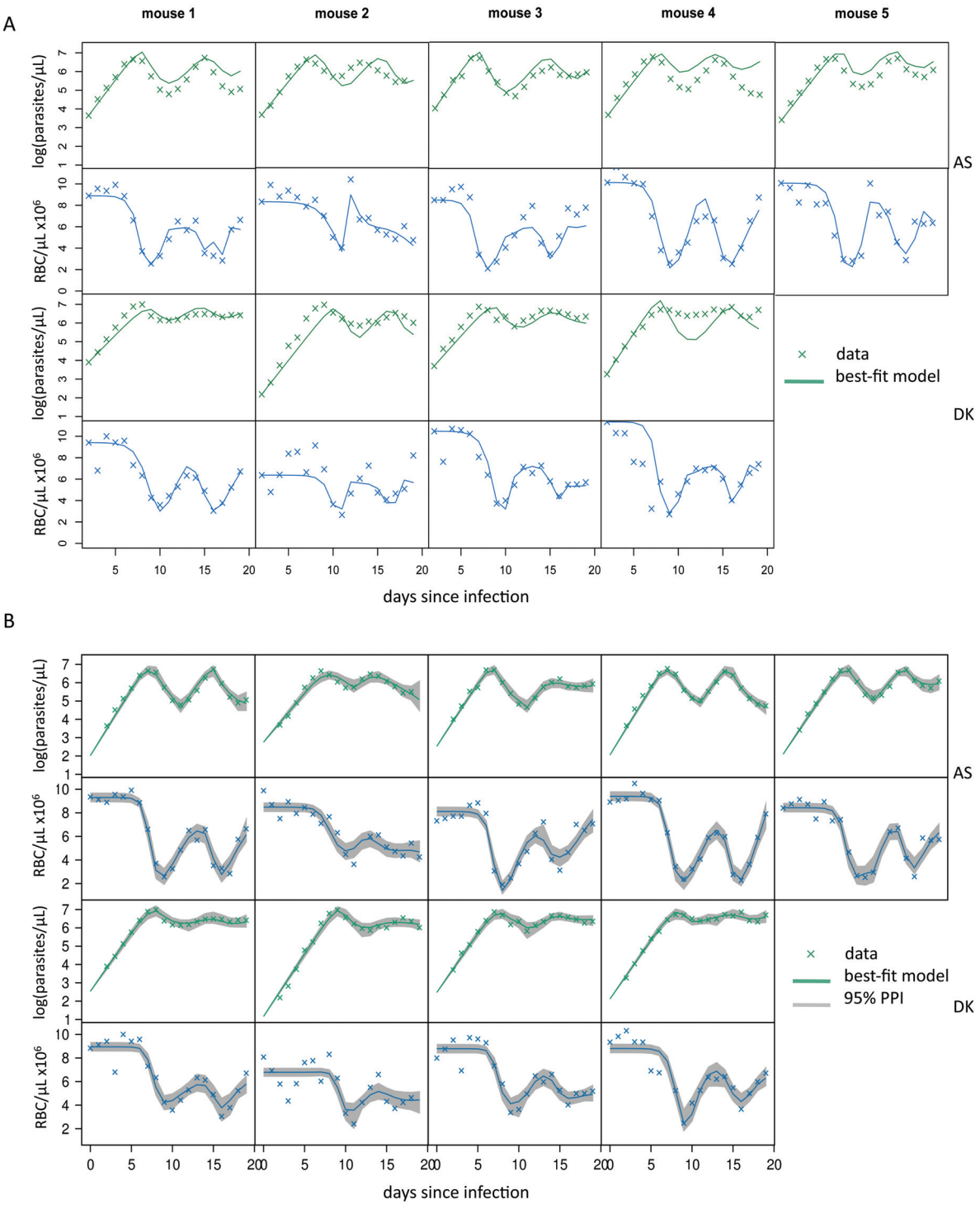

Figure B7: Comparison of model fits. *A*, Original best fit of red blood cell (RBC) age-structured model with no immunity, fitted to data from Barclay et al. (2008). Redrawn from Mideo et al. (2008*b*). *B*, Fit of hybrid model (including RBC age-structure and immune responses) to the same data set.

Table B1. Analysis of red blood cell (RBC) invasion rates in $CD4^+$-depleted mice

	LRT (χ^2)	*P*
Minimal model:		
RBC age	NA	
Genotype	NA	
Genotype : RBC age	$\chi^2_1 = 8.234$	.004
Nonsignificant terms deleted from maximal model:		
Mass of mouse	$\chi^2_1 = .380$	.538

Note: LRT = likelihood ratio test; NA = not applicable.

Table B2. Analysis of burst sizes in $CD4^+$-depleted mice

	F	*P*
Minimal model:		
Genotype	$F_{1,15} = 11.021$	.005
Phenylhydrazine	$F_{1,15} = 4.067$	.062
Nonsignificant terms deleted from maximal model:		
Mass of mouse	$F_{1,14} = .893$	.361
Parasite density	$F_{1,13} = .181$	.677
Uninfected red blood cell density	$F_{1,12} = .317$	.584
Genotype : phenylhydrazine	$F_{1,11} = .975$	.345

Table B3. Comparing the fit of original model from Mideo et al. (2008*b*) with the Miller et al. (2010) model of the main text using Bayes factors (BFs)

Genotype	BF	Interpretation of BF
AS	1.1×10^{40}	AS data are overwhelming more likely under the Miller et al. (2010) model
DK	4.5×10^{-6}	DK data are overwhelmingly more likely under the Mideo et al. (2008*b*) model, suggesting that the Miller et al. (2010) model overfits the data
All	4.9×10^{36}	Conclusions are the same as those for the newly collected data: immune responses are important for explaining dynamics of more virulent (AS) but not for the less virulent (DK) genotype

 DOI: 10.1086/662670

Appendix A from N. Mideo et al., "Causes of Variation in Malaria Infection Dynamics: Insights from Theory and Data"

(Am. Nat., vol. 178, no. 6, p. 174)

Supplementary Methods

Effects of Experimental Manipulation

Some effects of our experimental manipulation of host immunity and RBC age structure can be seen in figure A1. Mean parasite densities for each treatment over the initial peak of infection are shown in figure A1, top row. As expected, parasite densities are higher in $CD4^+$ T-depleted mice than in immune-intact control mice (Barclay et al. 2008). Mean RBC densities for each treatment over the initial peak of infection are shown in figure A1, bottom row. PHZ treatment results in a marked decrease in RBC densities. Figure A2 illustrates that PHZ-treated mice had significantly higher proportions of bloodstream reticulocytes and that a significantly higher proportion of infected RBCs were reticulocytes, across the relevant days postinfection.

Model Derivation

Basic Structure

Incorporating the age structure of the Mideo et al. (2008*b*) model into the model of Miller et al. (2010) yields the following basic model structure. On the $(i+1)$th day postinfection, just after all infected red blood cells (RBCs) burst, the densities of merozoites, M_{i+1}, reticulocytes on their jth day in the bloodstream, $R_{j,i+1}$, and mature RBCs, N_{i+1} are given by

$$\begin{aligned}
M_{i+1} &= \omega_{\mathrm{R}} \sum_{j=1}^{3} R_{j,i}[\lambda_{\mathrm{R}} e^{(\lambda_{\mathrm{R}}+d+I_{\mathrm{p},i})} + (1-e^{-\lambda_{\mathrm{R}}})e^{-(d+d_2+I_{\mathrm{p},i})}] \\
&\quad + \omega_{\mathrm{N}} N_i[\lambda_{\mathrm{N}} e^{(\lambda_{\mathrm{N}}+d+I_{\mathrm{p},i})} + (1-e^{-\lambda_{\mathrm{N}}})e^{-(d+d_2+I_{\mathrm{p},i})}], \\
R_{1,i+1} &= [\theta(K-T_{i-r}) + dK]\frac{1-e^{-(d+I_{\mathrm{u},i})}}{d+I_{\mathrm{u},i}}, \\
R_{2,i+1} &= R_{1,i} e^{-(\lambda_{\mathrm{R}}+d+I_{\mathrm{u},i})}, \\
R_{3,i+1} &= R_{2,i} e^{-(\lambda_{\mathrm{R}}+d+I_{\mathrm{u},i})}, \\
N_{i+1} &= R_{3,i} e^{-(\lambda_{\mathrm{R}}+d+I_{\mathrm{u},i})} + N_i e^{-(\lambda_{\mathrm{N}}+d+I_{\mathrm{u},i})},
\end{aligned}$$

where ω_{R} and ω_{N} are the number of progeny parasites produced in infected reticulocytes and mature RBCs, respectively, K is the normal total RBC density in the absence of infection and natural death, θ is the proportion of any RBC deficit that is made up in one day (and describes how RBC production increases with anemia; we therefore refer to it as the "upregulation rate"), d is the natural death rate of RBCs, d_2 is the additional death rate of multiply-parasitized RBCs and $T_{i-\tau} = \sum_{j-1}^{3} R_{j,i-\tau} + N_{i-\tau}$ is the total RBC density τ days before i. The parameter τ allows RBC production in response to anemia to be time-lagged, since RBC precursors take time to develop in the bone marrow. The parameters $I_{\mathrm{p},i}$ and $I_{\mathrm{u},i}$ describe the immune clearance rates of parasitized and unparasitized RBCs as a function of time i. These parameters are described in more detail below. The parameters λ_{R} and λ_{N} define the average number of merozoites (that survive clearance in the bloodstream) per reticulocyte

and mature RBC, respectively. To find expressions for these parameters, we note that an individual merozoite has a probability of infecting a reticulocyte given by

$$\frac{\beta_{\mathrm{R}} \sum_{i=1}^{3} R_{j,i}}{\beta_{\mathrm{R}} \sum_{j=1}^{3} R_{j,i} + \beta_{\mathrm{N}} N_i + \mu + I_{\mathrm{m},i}},$$

and an individual merozoite has a probability of infecting a mature RBC given by

$$\frac{\beta_{\mathrm{N}} N_i}{\beta_{\mathrm{R}} \sum_{j=1}^{3} R_{j,i} + \beta_{\mathrm{N}} N_i + \mu + I_{\mathrm{m},i}},$$

where β_{R} and β_{N} are the invasion rates of reticulocytes and mature RBCs, μ is the death rate of merozoites in the bloodstream, and $I_{\mathrm{m},i}$ describes the immune clearance rate of merozoites as a function of time, i. Multiplying these probabilities by the initial density of merozoites and dividing by the respective densities of RBCs gives the average number of merozoites per reticulocyte:

$$\lambda_{\mathrm{R}} = \frac{\beta_{\mathrm{R}} M_i}{\beta_{\mathrm{R}} \sum_{j=1}^{3} R_{j,i} + \beta_{\mathrm{N}} N_i + \mu + I_{\mathrm{m},i}}$$

and the average number of merozoites per mature RBC

$$\lambda_{\mathrm{N}} = \frac{\beta_{\mathrm{N}} M_i}{\beta_{\mathrm{R}} \sum_{j=1}^{3} R_{j,i} + \beta_{\mathrm{N}} N_i + \mu + I_{\mathrm{m},i}}.$$

The probability of a reticulocyte being infected by k merozoites is Poisson distributed with parameter λ_{R} and the probability of a mature RBC being infected by k merozoites is Poisson distributed with parameter λ_{N} (Miller et al. 2010). See Miller et al. (2010) for further details on the derivation of the model without age structure.

The model of Mideo et al. (2008*b*) discussed in the main text is recovered by setting all immune clearance parameters ($I_{\mathrm{m},i}$, $I_{\mathrm{p},i}$, and $I_{\mathrm{u},i}$) to 0. This is slightly different than the published model in Mideo et al. (2008*b*) since it tracks infections in time steps of thirds of a day rather than whole days and multiply infected RBCs are tracked separately. This allows the model to make predictions about the densities of unparasitized, singly parasitized, and multiply parasitized cells that should more accurately correspond to what is measured experimentally. However, all underlying biological hypotheses described by the model remain unchanged.

Immune Clearance

Three independent functions describe the immune clearance rates of merozoites, parasitized RBCs, and unparasitized RBCs over the course of infection (denoted $I_{\mathrm{m},i}$, $I_{\mathrm{p},i}$, and $I_{\mathrm{u},i}$). We assume that there are at maximum two "windows" of immune activity, and each window is described by four parameters (so each function is fully described by eight parameters). A schematic "clearance rate function" for parasitized RBCs is given in figure 1 of the main text. The parameter s_x defines the day postinfection when immune clearance begins, c_x represents the maximum clearance rate, r_x represents the time it takes to reach that maximum rate (or "rise time"), and l_x represents the duration of immune clearance (note that $r_x \leq l_x$). The subscript x denotes the cells being cleared (either m for merozoites, p for parasitized RBCs, or u for unparasitized RBCs). For each immune clearance function, the two windows of immune activity will be described by a different set of parameters.

Model Fitting

The fitted model parameters and prior distributions are given in table A1. The prior distributions were either taken from the literature or based on our experimental measurements. The prior distributions for burst size, RBC upregulation rate, and invasion rate are specified with hyperparameters (table A2); hyperparameters essentially specify the distribution from which the individual-level parameters are randomly drawn. We do this for these parameters because we want to examine if they are parasite genotype-specific (see below).

As well as fitting the hybrid model (Mideo et al. 2008*b*; Miller et al. 2010) with age structure and immune responses, we fit a model without age structure (Miller et al. 2010) by setting reticulocyte and normocyte burst sizes and invasion rates equal ($\omega = \omega_{\mathrm{N}} = \omega_{\mathrm{R}}$, $\beta = \beta_{\mathrm{N}} = \beta_{\mathrm{R}}$) and a model without immune responses (Mideo et

al. 2008*b*) by setting immune-mediated clearance rates to 0 ($c_m = c_p = c_u = 0$). We also fit models without age structure and with each of the three immune components removed by setting their respective clearance rates to 0.

Miller et al. (2010) showed that there is a nonidentifiability between RBC invasion rate β and natural death rate of merozoites μ. This meant that it was impossible to obtain separate estimates for them and all that could be obtained was their ratio. In Mideo et al. (2008*b*), however, we did not fit μ but assumed it had a value of 48 d^{-1}; thus, an estimate for β was obtainable. In order to test for genotype-specific differences in invasion rates we must therefore fix μ and assume that it is non-genotype-specific. Miller et al. (2010) estimated μ/β to be of the order 10^6, taking $\mu = 48$ as in Mideo et al. (2008*b*) gives β^{-1} to be of the order 10^4. The inverse of β is estimated rather than β because we have no prior knowledge about its upper bound.

In order to determine if there are genotype-specific differences in parameters we estimate the hyperparameters of the two strains in the model without age structure. For example, the prior distribution of burst size for AS-infected mice is $N(\nu_{\omega,\mathrm{AS}}, \sigma_\omega^2)$ and for DK-infected mice $N(\nu_{\omega,\mathrm{DK}}, \sigma_\omega^2)$. Terms $\nu_{\omega,\mathrm{AS}}$, $\nu_{\omega,\mathrm{DK}}$, σ_ω^2 are hyperparameters that we estimate. If there are genotype specific differences in parameter estimates we expect to see a difference in the posterior distributions of $\nu_{\omega,\mathrm{AS}}$ and $\nu_{\omega,\mathrm{DK}}$, that is, the mean burst sizes of mice infected with AS and DK parasites, respectively. The variance hyperparameter σ_ω^2, is assumed to be non-strain-specific as it is of little interest here. We can also suppose that the burst sizes for all mice are randomly drawn from the same population, that is, non-strain-specific burst sizes, which means we take the prior as $N(\nu_\omega, \sigma_\omega^2)$ over all mice. We must also specify hyperpriors on the hyperparameters; these are given in table A2 and are chosen to be conjugate to the priors.

By estimating genotype-specific and non-genotype-specific hyperparameters we can calculate the (marginalized) likelihood ratio of the data supposing genotype-specific hyperparameters to the data supposing non-genotype-specific hyperparameters. Without any prior preference for these two suppositions their prior odds are 1 : 1. Thus, by Bayes's theorem, our posterior odds for these suppositions are equal to their likelihood ratio. If $\Pr(D_m|M)$ is the likelihood of mouse m's data given model M, then our odds on genotype-specific hyperparameters is given by the ratio

$$\frac{\Pi_m \Pr(D_m|\text{genotype-specific hyperparameters})}{\Pi_m \Pr(D_m|\text{nongenotype-specific hyperparameters})}.$$

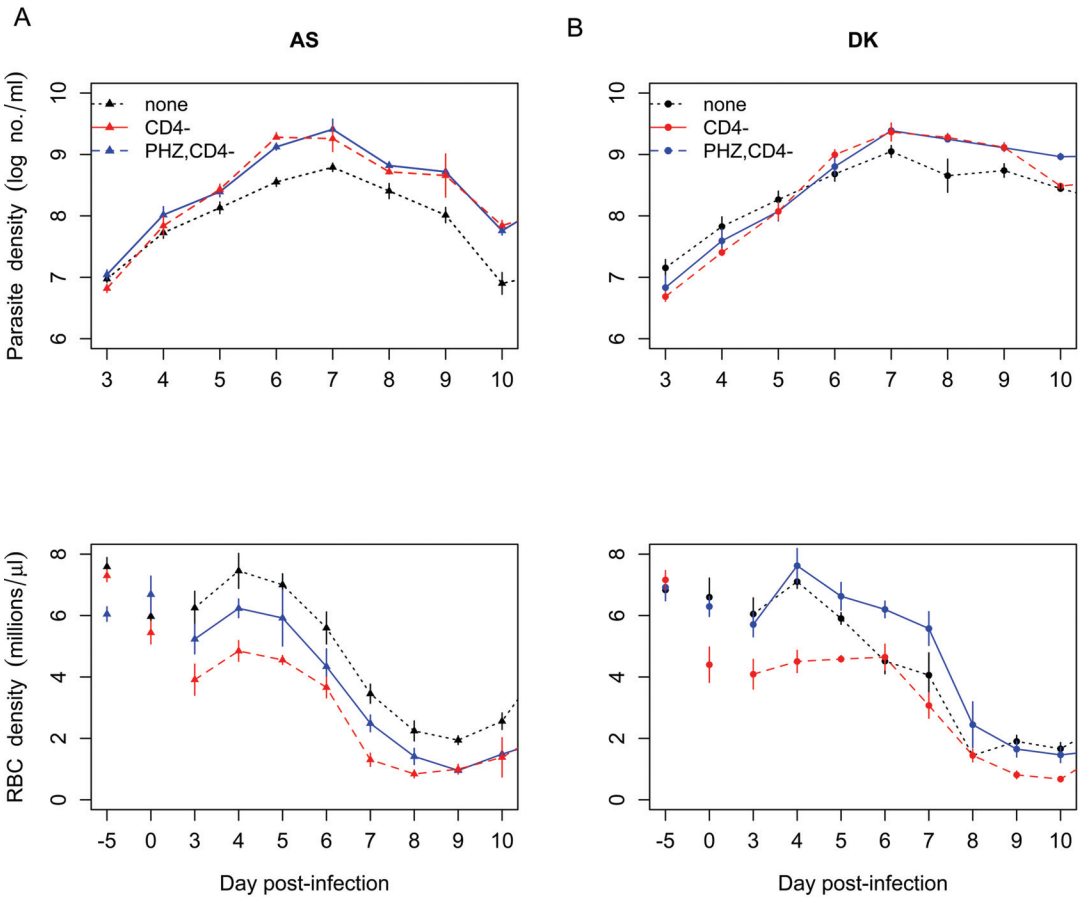

Figure A1: Infection dynamics of different treatments. Treatments are grouped by parasite genotype: *A*, More virulent parasite genotype AS; *B*, less virulent parasite genotype DK. Top row shows mean parasite density, and bottom row shows mean RBC densities over time. Error bars, ± 1 SEM. Colors indicate what treatments in addition to infection the hosts received: black, none (immune-intact control); blue, $CD4^+$ depletion (CD4−); red, PHZ and $CD4^+$ depletion. Over the course of the initial peak, parasite densities were higher in $CD4^+$-depleted hosts as compared with immune-intact hosts. PHZ treatment (2 days before infection, i.e., day -2) resulted in a decrease in red blood cell densities. This effect coincided with the initial stages of infection.

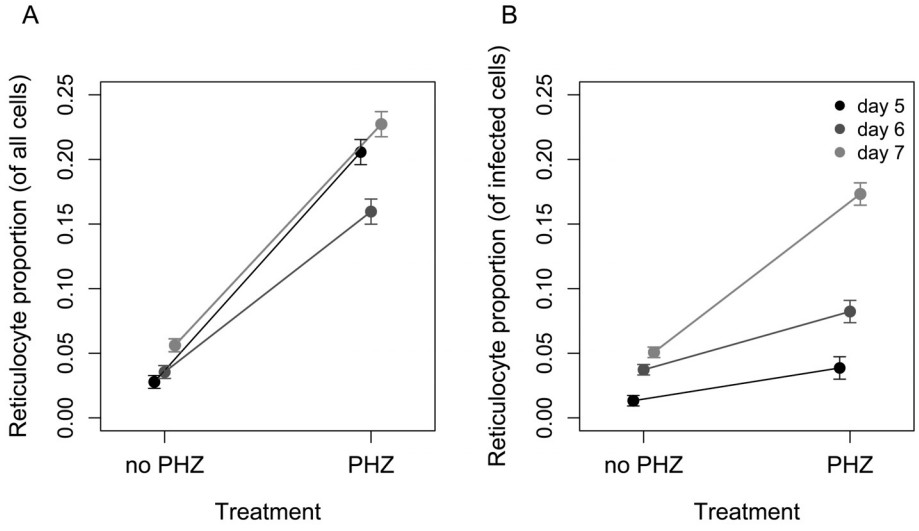

Figure A2: Effect of phenylhydrazine (PHZ) on red blood cell age structure in $CD4^+$ depleted mice. The mean proportion of all red blood cells (RBCs) that are reticulocytes (*A*) and infected RBCs that are reticulocytes (*B*) over 3 consecutive days in untreated mice and those that received PHZ treatment. Error bars, ± 1 SEM. At the early stages of infection, mice treated with PHZ had a significantly higher proportion of reticulocytes, as expected, and subsequently, a significantly higher proportion of all infected cells were also reticulocytes.

Table A1. Model parameters and prior distributions of hybrid model

Parameter	Description	Value or prior	Source
ω_R, ω_N	Burst sizes in reticulocytes and normocytes	$N(\nu_\omega, \sigma_\omega^2)$	See table A2
β_R, β_N	Invasion rate of reticulocytes, normocytes ([cells/μL]$^{-1}$ s^{-1})	Not fitted	
ρ	$\log_{10}(\beta_R/\beta_N)$	$N(0, .3^2)$	Hetzel and Anderson 1996; Antia et al. 2008; Mideo et al. 2008*b*
μ	Natural death rate of merozoites (day^{-1})	48	Garnham 1966; Mideo et al. 2008*b*
β^{-1}	Inverse of invasion rate (cells s/μL)	Exp(l)	See table A2
θ	Rate of upregulation of erythropoeisis (day^{-1})	$N(\nu_\theta, \sigma_\theta^2)$	See table A2
τ	Time lag in erythropoeisis (day)	$U(0, 6)$	Chang et al. 2004; Mideo et al. 2008*b*
d	Natural death rate of RBCs (day^{-1})	.025	van Putten 1958; Bannerman 1983
d_m	Increased death rate of multiply-parasitized RBCs (day^{-1})	Exp(1)	Miller et al. 2010
s_m, s_p, s_u	Start day of immunity targeting merozoites, parasitized RBCs, unparasitized RBCs	$U(0, 21)$	Miller et al. 2010
r_m, r_p, r_u	Rise time of immunity targeting merozoites, parasitized RBCs, unparasitized RBCs	$U(0, 21)$	Miller et al. 2010
c_m	Maximum level of immunity targeting merozoites (cells/s)	Exp(10^8)	Miller et al. 2010
c_p, c_u	Maximum clearance rate of immunity targeting parasitized RBCs, unparasitized RBCs (day^{-1})	Exp(1)	Miller et al. 2010
l_m, l_p, l_u	Duration of immunity targeting merozoites, parasitized RBCs, unparasitized RBCs	$U(0, 21)$	Miller et al. 2010
P_0	Initial parasite density (parasites/μL)	$\log N(1.5, .5^2)$	Miller et al. 2010
N_0	Initial RBC density (RBCs/μL)	$N_T(6.5 \times 10^6, 10^{12})$	

Note: RBC = red blood cell.

Table A2. Hyperparameters and their hyperprior distributions.

Hyperparameter	Description	Hyperprior	Source
ν_ω	Mean burst size	$N(6, .5^2)$	Garnham 1966; Carter and Walliker 1975; Carter and Diggs 1977; Mideo et al. 2008*b*
σ_ω^2	Variance of burst size	InvGam(2, 1^2)	Garnham 1966; Carter and Walliker 1975; Carter and Diggs 1977; Mideo et al. 2008*b*
ν_β	Mean inverse invasion rate	InvGam(1, 10^4)	Mideo et al. 2008*b*
ν_θ	Mean red blood cell upregulation rate	$N(0.4, 0.2^2)$	Haydon et al. 2003; Mideo et al. 2008*b*
σ_θ^2	Variance of red blood cell upregulation rate	InvGam(2, 0.2^2)	Haydon et al. 2003; Mideo et al. 2008*b*